IEEE Photonics Journal
An IEEE Photonics Society Publication

Open Access

LCoS-Based Wavelength-Selective Switch for Future Finer-Grid Elastic Optical Networks Capable of All-Optical Wavelength Conversion

Volume 9, Number 2, April 2017

Dequan Xie
Danshi Wang
Min Zhang
Zichen Liu
Quan You
Qi Yang
Shaohua Yu

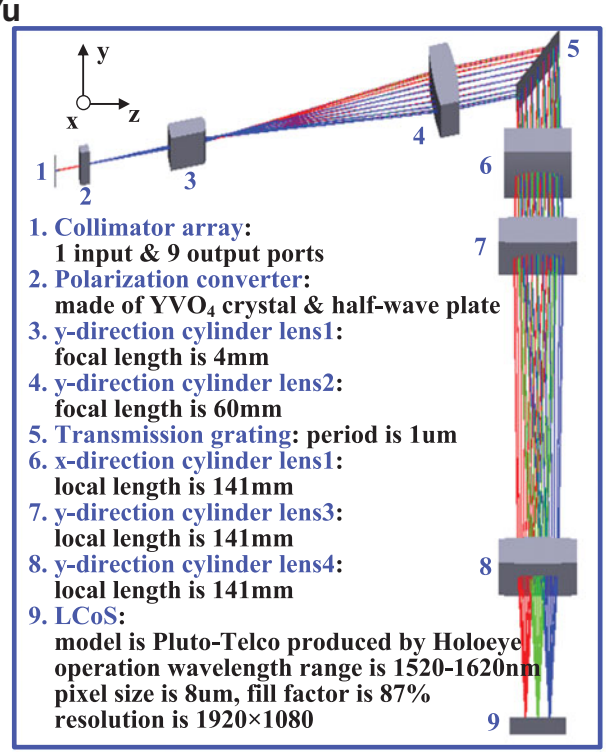

(a)

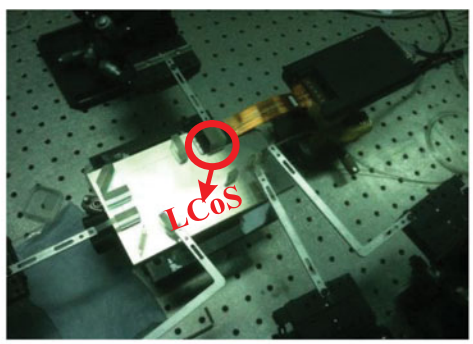

(b)

(c)

DOI: 10.1109/JPHOT.2017.2671436
1943-0655

IEEE photonics SOCIETY

IEEE

LCoS-Based Wavelength-Selective Switch for Future Finer-Grid Elastic Optical Networks Capable of All-Optical Wavelength Conversion

Dequan Xie,[1,3] Danshi Wang,[2] Min Zhang,[2] Zichen Liu,[3] Quan You,[3] Qi Yang,[3] and Shaohua Yu[3]

[1]Wuhan National Laboratory for Optoelectronics, School of Optical and Electronic Information, Huazhong University of Science and Technology, Wuhan 430074, China
[2]State Key Laboratory of Information Photonics and Optical Communications, Beijing University of Posts and Telecommunications, Beijing 100876, China
[3]State Key Laboratory of Optical Communication Technologies and Networks, Wuhan Research Institute of Posts and Telecommunications, Wuhan, Hubei, 430074, China

DOI:10.1109/JPHOT.2017.2671436

Manuscript received November 22, 2016; revised February 15, 2017; accepted February 15, 2017. Date of publication February 17, 2017; date of current version March 8, 2017. This work was supported by the National Natural Science Foundation of China under Project 61372119, the Doctoral Scientific Fund Project of the Ministry of Education of China (20120005110010), and the BUPT Excellent Ph.D. Students Foundation (CX2015306). Corresponding author: D. Wang (e-mail: danshi_wang@bupt.edu.cn).

Abstract: A finer-grid wavelength-selective switch (WSS) based on liquid crystal on silicon is proposed, fabricated, and demonstrated. Based on the cost-effective method, namely combined lenses technique, the focal length is increased so that both the bandwidth setting resolution and grid granularity is improved from 12.5 to 6.25 GHz compared with the conventional WSS. To demonstrate its utility, we apply this finer-grid WSS to a reconfigurable optical add/drop multiplexer structure and an all-optical wavelength conversion (AOWC) module. To enable a finer-grid WSS, the performance of a finer-grid elastic optical network (EON) capable of AOWC is also investigated. Different from the conventional AOWC scheme for fixed-grid WDM networks, we propose and experimentally demonstrate a four-wave-mixing-based AOWC module specifically for EON. In addition to physical experiments, an optical network's control and management scheme corresponding to the designed physical scenario is also investigated. Experimental and simulation results show that the proposed method achieves higher spectrum efficiency, lower blocking probability, finer switching granularity, and higher conversion resolution.

Index Terms: Liquid-crystal devices, optical switching devices, elastic optical network, nonlinear optical signal processing.

1. Introduction

Recently, liquid crystal on silicon (LCoS) has opened up new possibilities for the use of liquid crystal, with potential applications in various fields [1]. The high resolution and fast response of LCoS techniques have led to numerous applications in optics: For example, a mode converter has been employed on an LCoS-based spatial light modulator [2]; a low-voltage polymer-stabilized structure for LCoS-based phase-only modulation has been investigated [3]; and a compact LCoS-based wavelength blocker array has been presented [4]. In particular, LCoS-based wavelength selective switches (WSSs) are considered to be key factors in future optical networks [5].

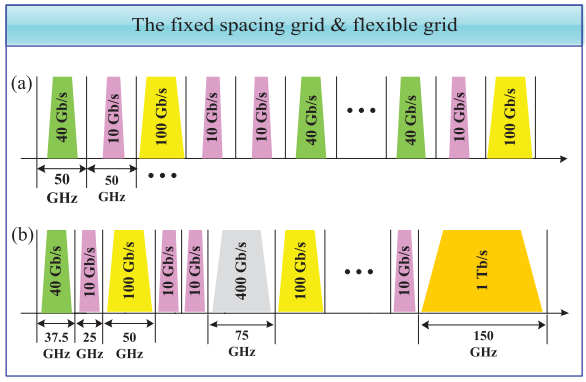

Fig. 1. (a) Traditional WDM networks with fixed spacing grid (50 GHz). (b) Elastic optical networks with flexible grid (12.5 GHz).

WSSs are at the heart of reconfigurable optical add/drop multiplexer (ROADM) structure, which is a key nodal subsystem in next-generation wavelength division multiplexing (WDM) networks. Traditional WDM networks strictly follow the ITU-T wavelength grids and spacing. Nonetheless, the standard ITU-T grids with fixed spacing (i.e., 50 GHz) are coarse, resulting in a significant waste of optical spectra and limited potential to improve the transmission capacity [6], as shown in Fig. 1(a). Therefore, elastic optical networks (EONs) have been developed that can dynamically allocate a flexible amount of spectral resources to individual channels to support heterogeneous line rates [7], as shown in Fig. 1(b). Accordingly, ITU-T revised the latest G.694.1 standard, which describes the concept of a flexible grid and defines the frequency slot width as 12.5 GHz [8]. This has encouraged the development of hardware facilities such as 12.5 GHz-grid bandwidth-variable WSS (BV-WSS), which can route the incoming optical signals with different optical bandwidths and central wavelengths to any output fiber [9].

With the exponential growth of network capacity and traffic rates, data traffic grooming is becoming increasingly important as a means of further improving the efficiency and flexibility of networks. To better utilize optical spectrum resources, finer-grid granularity for next-generation EON (NG-EON) is desired. However, the continued use of 12.5 GHz grids by commercial BV-WSS blocks the development of finer-grid ROADM for NG-EON. The finer grids can be achieved by adopting the higher-resolution LCoS, such as waveshaper [10], but the extremely high cost makes it impractical for NG-EON. Hence, it is important to develop the cost-effective technique for WSS to achieve finer grids.

In addition, to further increase the network efficiency and decrease the blocking probabilities, the wavelength conversion (WC) function is needed to avoid wavelength contention for dynamic optical path switching at the nodes [11]. Traditionally, WC has been performed by a transponder at each node, whereby a signal is dropped, received, and transmitted at a different wavelength. However, transponders basically work with specific modulation formats and symbol rates, limiting the flexibility of the network's operation. The all-optical wavelength conversion (AOWC) technique without optical-electrical-optical (OEO) conversions, particularly that based on four-wave mixing (FWM) effect in a semiconductor optical amplifier (SOA), represents a promising choice for WC, as it offers transparent modulation formats, ease of integration, and ultra-high processing speed [12]–[14], but the reported AOWC schemes are mainly employed in the fixed grid optical networks, but not in EONs. So far, there are few studies having been done to provide the solution for EON with the ability of WC.

In this paper, a novel ROADM structure based on finer-grid WSS with AOWC module is proposed for NG-EON. We have researched and fabricated a 1×9 finer-grid WSS based on LCoS. Compared with the commercial BV-WSS, the frequency slot width is refined from 12.5 GHz to 6.25 GHz. The model and principle of WSS are analyzed in detail. Based on the combined lenses technique,

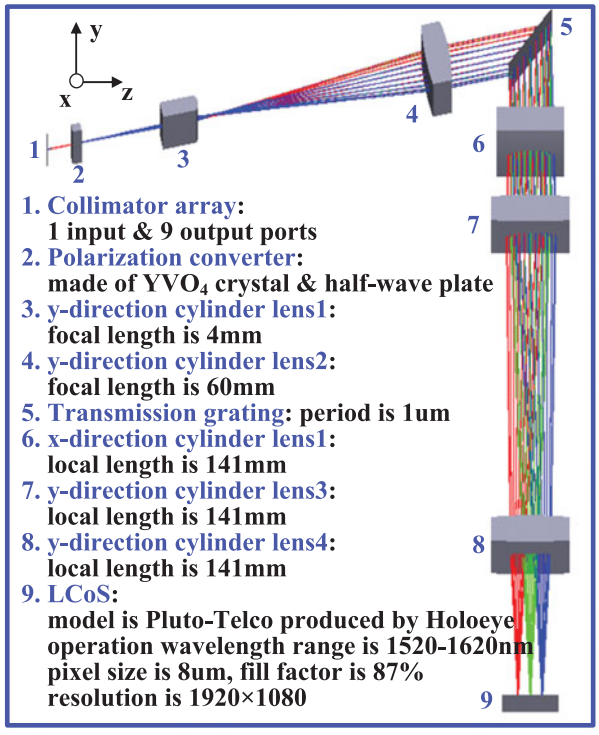

(a)

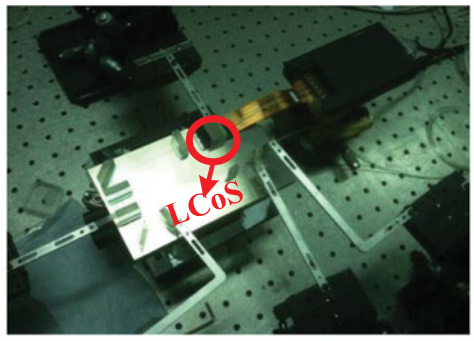

(b)

(c)

Fig. 2. (a) Schematic diagram of a finer-grid WSS based on LCoS. (b) Internal optical path structure. (c) Real product photo of a packaged finer-grid WSS.

the focal length is increased so that both the bandwidth setting resolution and grid granularity is improved but without cost growth. Moreover, with the help of this cost-effective and high-performance WSS, we are able to implement an AOWC module based on FWM in an SOA. Signals in different modulation formats, such as DPSK, QPSK, and 16QAM, are comprehensively investigated. In addition to the physical experiments, we also study the optical network's control and management scheme corresponding to the designed physical scenario. In summary, our proposed scheme can effectively improve the spectrum efficiency, decrease the blocking probability, and optimize the network performance.

2. Finer-Grid Wavelength-Selective Switch

The schematic of finer-grid WSS based on LCoS is shown in Fig. 2(a), in which each component and their detailed information are also listed. In the wavelength distribution direction (y-axis), the optical signals are fed into the system via the collimator array. Since the LCoS is sensitive to polarization, the random-polarization light is converted into extraordinary light (e light) by the polarization converter. A pair of anamorphic condenser lenses (y-direction lens1 and lens3) are employed as a beam expander to change the beam waist to an appropriate form on the transmission grating surface. Through the grating, the optical signals at different wavelengths are output at different angles. After the other y-direction condenser lens, each wavelength can be focused onto the corresponding pixel area of the LCoS. The phase of each pixel is controlled by the digital driven mode based on pulse width modulation. By controlling the phase of pixels in the switching direction (x-axis), based on Fraunhofer effect, the optical signal at each wavelength can be reflected to the desired output port. The photos of internal optical path structure and packaged product are displayed in Fig. 2(b) and (c).

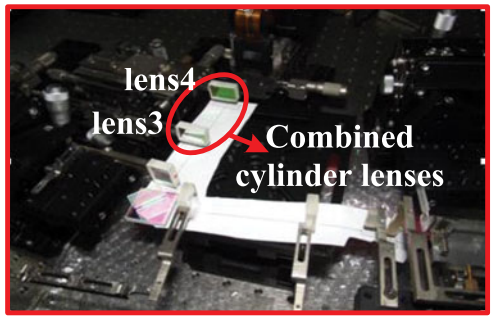

Fig. 3. Schematic of optical path setting for combined cylinder lenses.

Based on above-described configuration, the bandwidth setting resolution BW_{res} of WSS is

$$BW_{res} = \frac{d \times (\lambda\text{max} - \lambda\text{min})}{f \times \tan(\theta_{\lambda}\text{max} - \theta_{\lambda}\text{minx})} \tag{1}$$

where d is the pixel size of LCoS; f is the focal length of condenser lens in front of LCoS; $\theta_{\lambda}\text{max}$ and $\theta_{\lambda}\text{min}$ are the output angles from the grating, corresponding to the maximum wavelength λmax and minimum wavelength λmax, respectively.

In our work, the λmax is 1570 nm and λmin is 1530 nm so that the $\lambda\text{max} = 53.6^{\circ}$ and $\lambda\text{min} = 49.9^{\circ}$. According to (1), it is seen that BW_{res} is mainly dependent on the parameters f and d. In order to achieve finer bandwidth setting resolution and grid granularity, the value of BW_{res} should be decreased. Obviously, there are two methods: decreasing the pixel size of LCoS d, or increasing the focal length of condenser lens f. However, due to the extremely high cost, higher-resolution LCoS-based WSS cannot be widely applied for practical EON, such as Finisar waveshaper, which is mainly used as a narrow-band tunable filter in the lab but not a switching module in ROADM. Moreover, the small pixel-size LCoSs not only increase the cost significantly, but also may cause the electric field crosstalk among pixels. Hence, different from the existing technique, we propose the other more cost-effective and practical method: keeping the pixel size of LCoS unchanged, but increasing the focal length f. In addition, in the conventional WSS, the condenser lens is single, which means the single lens has to be customized for the required focal length, and focal length is nonadjustable. Here, we propose a combined lenses structure instead of single lens, consisting of y-direction cylinder lens3 and lens4, as shown in Fig. 3. The advantage of our technique is that the focal length of combined lenses can be adjusted flexibly by changing the distance between lens3 and lens4, without damaging the aberration nor increasing additional cost. We adopt the LCoS produced by Holoeye Corp, and its pixel size d is 8 um. Based on the precise design, the distance between lens3 and lens4 is set as 78 mm, and thus, the focal length f is 98 mm to realize the 6.25 GHz bandwidth setting resolution.

A test system consisting of a tunable laser (Agilent 81960A), polarization controller, multi-port optical meter (Agilent N7745A), and lightwave measurement analyzer (Agilent 8164B) is used to investigate the performance of finer-grid WSS, including the insertion loss (IL), port isolation, minimum bandwidth, bandwidth setting resolution, polarization-dependent loss (PDL), and differential group delay (DGD). All nine ports have the similar performance, and thus we take Port 1 as the test reference, as shown in Fig. 4(a). The IL range of Port 1 is 5.5-6 dB across the entire C-band (1530-1570 nm). The ripples in the transmission spectra are caused by the gap between the pixels on the LCoS. Narrower gaps can suppress the ripples and reduce the IL nonuniformity. The port isolation for each port is larger than 25 dB, which effectively mitigates the interference from other ports. The tunable bandwidth is displayed in Fig. 4(b). The bandwidth can be flexibly adjusted by the programmable software. The center wavelength is fixed at 1550 nm, and the 3 dB passband bandwidths range from 15 GHz to 1 THz. The maximum bandwidth can reach 5 THz across the entire C-band.

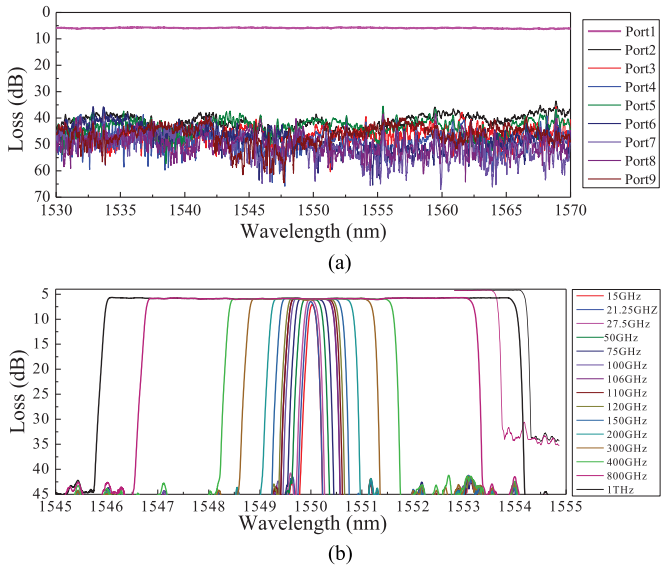

Fig. 4. (a) Measured insertion loss and port isolation of the Port1. (b) Function of tunable bandwidth at the center wavelength of 1550 nm.

Next, we demonstrate the higher bandwidth setting resolution and finer grid granularity. The bandwidth can be digitally tuned at a resolution of 6.25 GHz, as displayed in Fig. 5(a), which enables the signal to vary its bandwidth more flexibly. The bandwidths are then fixed to 15 GHz, 25 GHz, 50 GHz, and 100 GHz. Under the different bandwidths, the center wavelengths can be tuned at steps of 6.25 GHz, enabling finer-grid granularity, as shown in Fig. 5(b)–(e). The finer slot granularity allows for finer switching ability in the ROADM. In addition, we measure the PDL and DGD of four random ports across the entire C-band. The PDL is less than 0.5 dB, and DGD is less than 1.4 ps, as shown in Fig. 6. The polarization dependent loss (PMD) is the average of DGD, and the value of PMD is less than 0.5 ps. Finally, the attenuation control range is 0 $\sim$ 15 dB, and attenuation setting resolution is 0.2 dB.

3. ROADM Structure Based on a Finer-Grid WSS Capable of AOWC

To subject our developed WSS to practical applications, we propose a scalable colorless, directionless, and contentionless (CDC) ROADM structure. Based on the finer-grid WSS, the CDC-ROADM can implement finer-granularity switching function for NG-EON, which can further improve spectrum utilization. Moreover, it is also equipped with a shared AOWC module in Fig. 7(a). The optical splitter distributes incoming channels from one degree to the drop portion of this degree and to the $1 \times N$ finer-grid WSSs of all other degrees. Each $1 \times N$ finer-grid WSS can select different services at different wavelengths with various bandwidths and route them to the corresponding destination nodes. To achieve a contentionless implementation, the $M \times N$ WSS must be able to switch any wavelength from any input port to any output port [15]. Currently, $M \times N$ WSS is not commercially available yet, but the function can be implemented using several smaller switches. Therefore, with the appropriate connection among these components, a CDC-ROADM can be successfully constructed.

However, in spite of the CDC characteristic, transmissions may still be blocked under the constraints of wavelength continuity, spectral continuity, and spectral conflict [11]. As shown in Fig. 8(a), in the fixed grid scenario without WC function, the service *B* at frequency *f* which intends to route from Note 1 to Node 4 has to be blocked because of the preoccupied frequency resource by service *C* between Node 3 and 4. To overcome this limitation, the wavelength converter, which can change the wavelength of a transit connection from one incoming wavelength to another wavelength, is

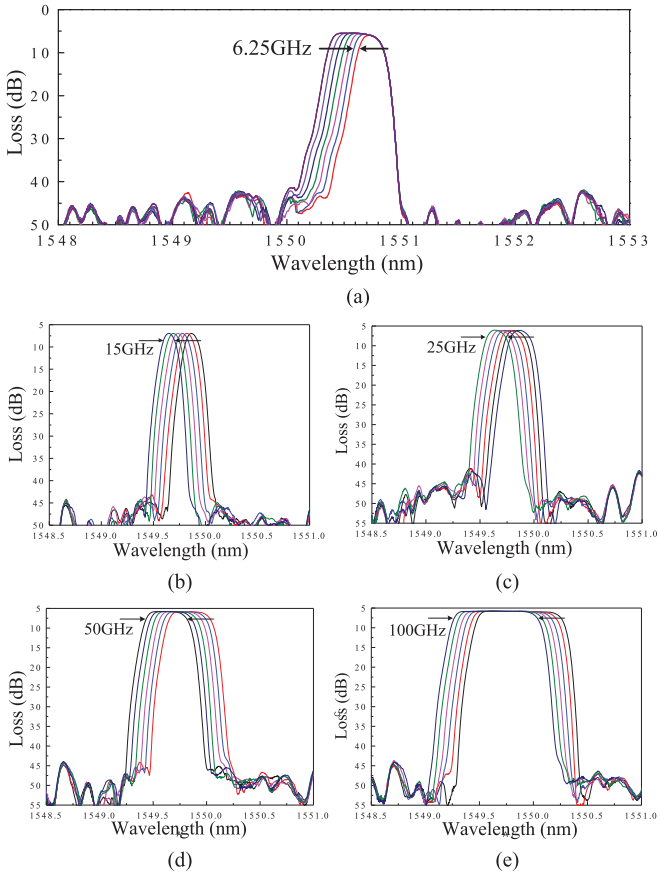

Fig. 5. (a) Measured bandwidth setting resolution: 6.25 GHz; the finer GHz grid granularity (6.25 GHz) for the fixed bandwidth of (b) 15 GHz, (c) 25 GHz, (d) 50 GHz, and (e) 100 GHz, respectively.

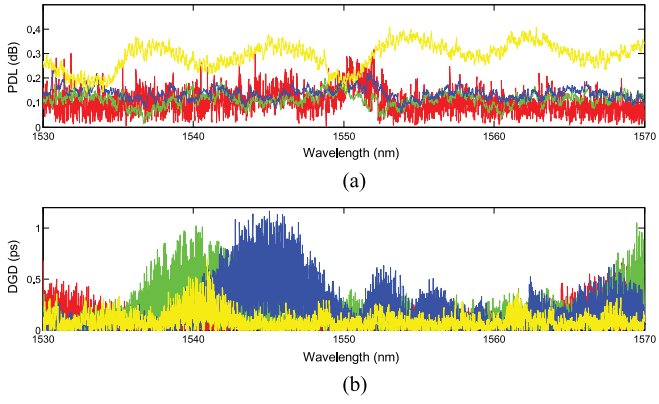

Fig. 6. (a) Measured PDL of four selected output ports. (b) Measured DGD of four output ports.

needed. Therefore, wavelength conflicts along the route of a channel can be resolved, and utilization of spectral resources can be increased, as shown in Fig. 8(b) [16]. However, the above referenced schemes with WC are all employed in the fixed grid optical networks but not in EONs. So far, there are few studies having been done to provide the solution for EON with the ability of WC. As shown in Fig. 8(c), in NG-EON, the node capable of WC can further increase the network efficiency and decrease the blocking probabilities.

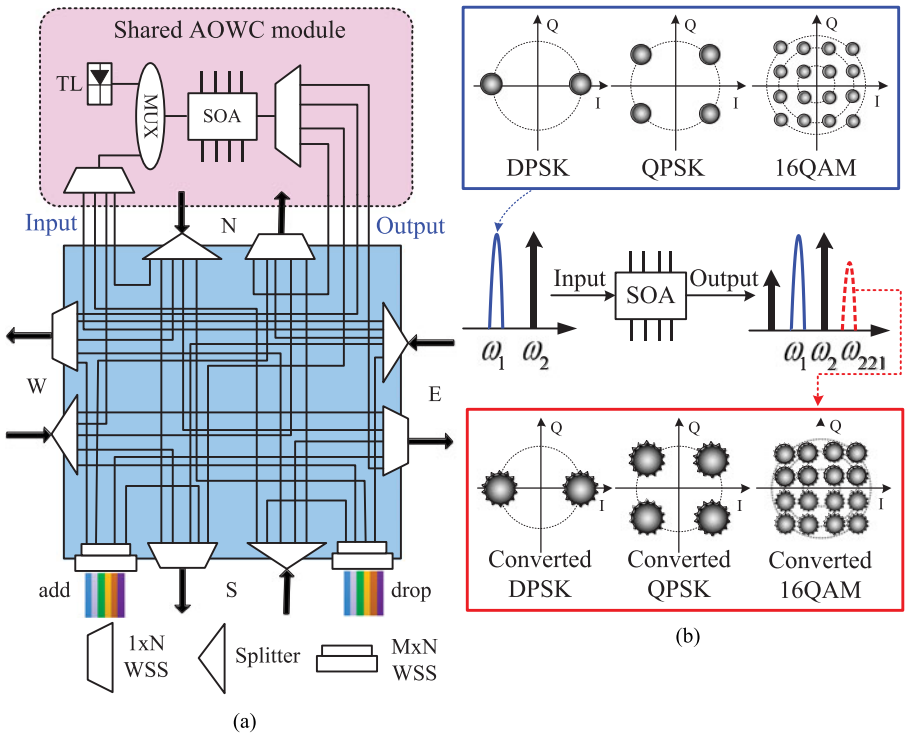

Fig. 7. (a) Scalable CDC-ROADM structure based on the finer-grid WSS and equipped with a shared AOWC module. (b) Operation principle of FWM in SOA for DPSK, QPSK, and 16QAM.

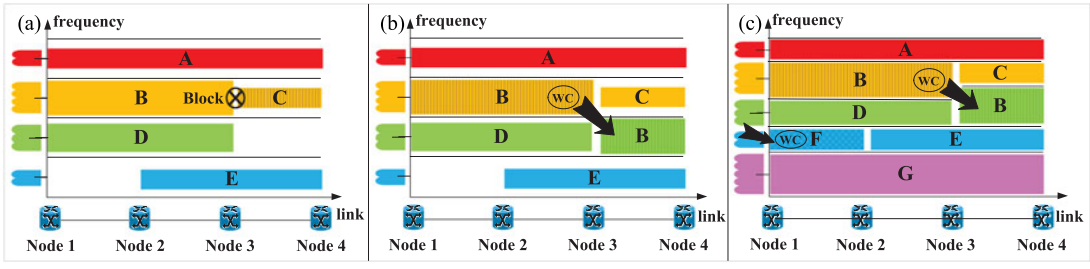

Fig. 8. (a) Fixed grid scenario without WC. (b) Fixed grid scenario with WC. (c) Flexible grid scenario with WC.

Therefore, aimed at NG-EON, we design a shared AOWC module based on the finer-grid WSS and SOA. Compared with other devices, the low cost, easy integration, and low input optical power of commercial SOAs makes them better suited to the ROADM structure. As shown in Fig. 7(a), the splitters from all directions are connected to one finer-grid WSS at the input port of the AOWC module. WC is not necessary for every input signal-it is only performed when the wavelengths conflict and the spectrum resources are insufficient. This WSS can select the desired wavelength that needs to be converted. The selected signal at ω_1 and the pump from a tunable laser (TL) at ω_2 are coupled together as the SOA input, as shown in Fig. 7(b). After FWM in SOA, the converted signal is generated at $\omega_{221} = 2\omega_2 - \omega_1$ [17]. Both the amplitude information and phase information of the original signal can be reserved and transparently transferred to the generated idler, which means that DPSK, QPSK, and 16QAM signals can implement the WC function. The converted signal is then demultiplexed by another WSS and routed to the destination port. In theory, the signal can be converted to any continuous wavelength by adjusting the frequency detuning between the pump and the original signal. However, in real optical networks, the converted signal has to be

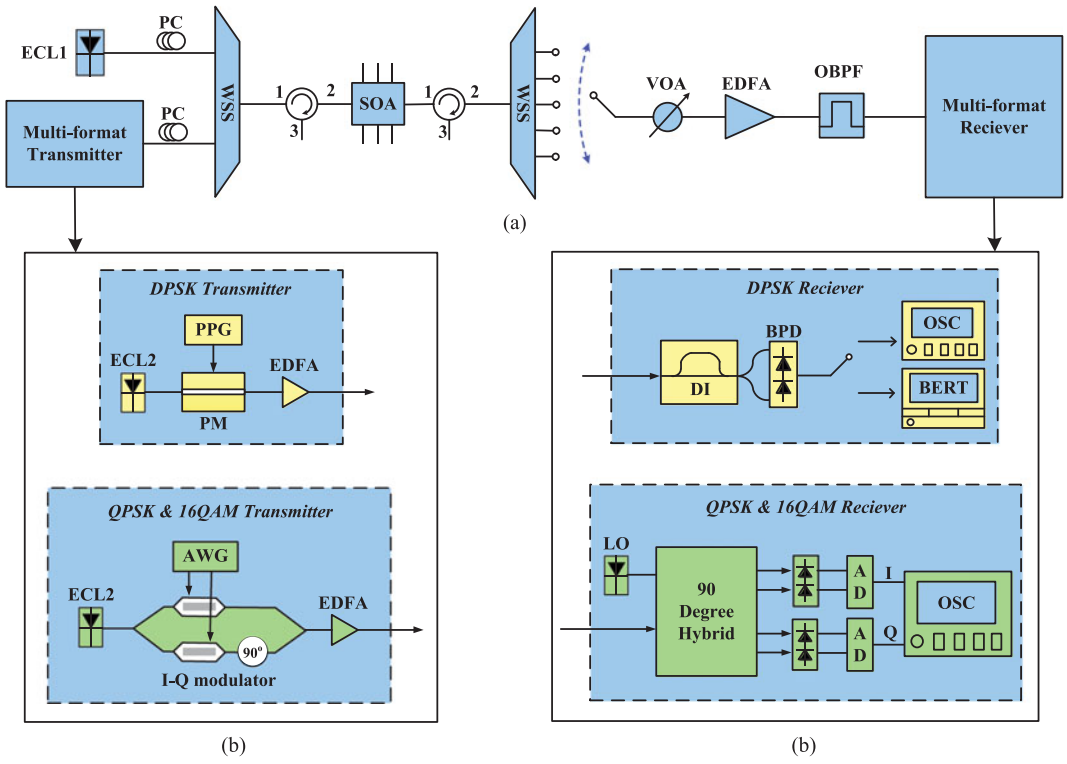

Fig. 9. Experimental setup: ECL: external cavity laser; PC: polarization controller; PPG: pulse pattern generator; PM: phase modulator; DI: delayed interferometer; BPD: balanced photonics detector; BERT: BER tester; AWG: arbitrary waveform generator; VOA: variable optical attenuator; EDFA: erbium-doped fiber amplifier; OBPF: optical band-pass filter; A/D: analog to digital converter; LO: local oscillation; OSC: oscilloscope.

allocated at the specified wavelength according to the WSS grid, because only the grid-aligned signal can be properly filtered. The finer-grid WSS can not only filter out the converted signal with flexible bandwidth but enable the finer-granularity conversion step as well.

4. Experimental Setup and Results

To demonstrate the feasibility of finer-grid WSS and AOWC module, we set up two physical experiment systems: the first one is based on phase modulator (PM), differential detection (DD), and BER tester (BERT) for DPSK signal; the other one is based on IQ modulator, coherent receiver, and off-line processing for QPSK and 16QAM signals (see Fig. 9). The original signals are generated from the multi-format transmitter consisting of two kinds of transmitters: DPSK signal is modulated by an optical PM which is driven by a pulse pattern generator (PPG Anritsu MP1800A) to provide the repeated pseudo-random binary sequence (PRBS) with a length of $2^{31} - 1$ at 12.5 Gbps; while QPSK and 16QAM signals are modulated by a IQ modulator (Tektronix OM5110) driven by an arbitrary waveform generator (Tektronix AWG7001A) to generate 25 Gbps QPSK signal and 50 Gbps 16 QAM signal, as shown in Fig. 9(b). The light sources of the pump and signal are from tunable external cavity lasers (ECL-EXFO-FLS2800) with linewidths of less than 100 kHz. The input signal and pump are multiplexed together by our finer-grid WSS. The combined input wavelengths are injected into the SOA (CIP-NL-OEC-1550) with a small gain of 34 dB and a saturation output power of 6 dBm. Two circulators, placed before and after the SOA, are used as isolators to avoid reflection interference. The relative polarization state between the pumps and the input signal can be controlled by the polarization controllers (PCs). After FWM, the generated

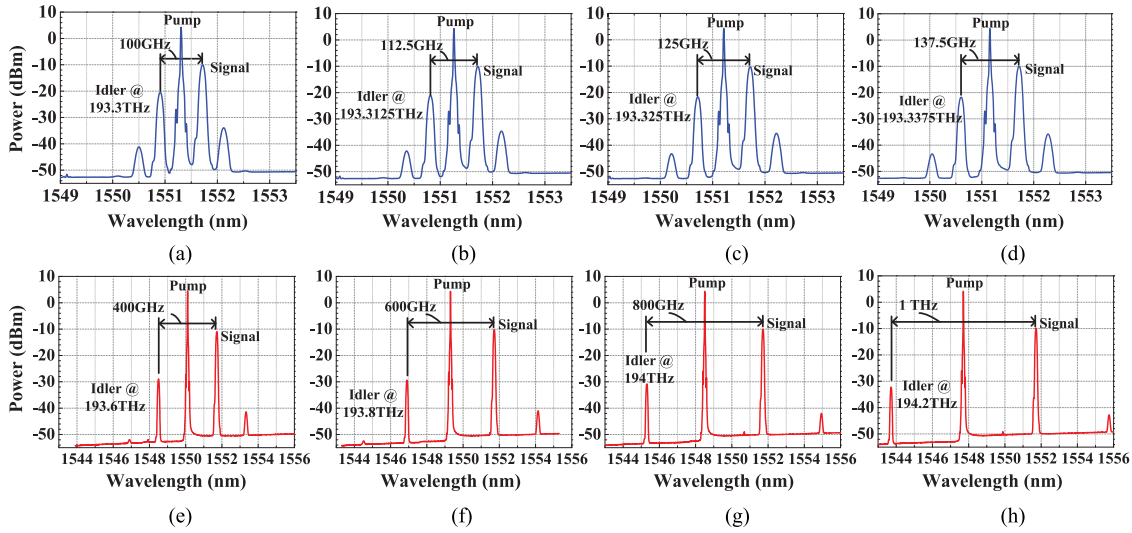

Fig. 10. Optical spectra of wavelength conversion based on FWM. (a)–(d) 12.5 GHz grid-aligned converted signals. (e)–(h) 200 GHz grid-aligned converted signals.

idlers are demultiplexed by the other finer-grid WSS, which can be controlled by the programmable software to filter the desired wavelengths and route to the destination port. The selected signal is detected by the multi-format receiver comprised of two kinds of receivers: the DPSK is demodulated by the Mach-Zehnder delayed-interferometer (DI) and detected by a balanced photonics detector (BPD-u2t-2150R); QPSK or 16QAM is detected by a coherent receiver (Tektronix OM4106D), as shown in Fig. 9(c). Here, the erbium-doped fiber amplifier (EDFA), operating as a pre-amplifier, is set to constant power mode to maintain the input power of the coherent receiver. Finally, the eye-diagrams of DPSK are obtained from an oscilloscope (OSC Agilent 86100A) and BERs are measured in real time by a BERT (MP1800A). On the other hand, for QPSK or 16QAM signals, the constellation diagrams and I/Q eye-diagrams are obtained by a 33-GHz OSC (Tektronix 73304DX), and the BER is calculated by the off-line processing. The optical spectra are observed by an optical spectra analyzer with a resolution of 0.05 nm (YOKOGAWA AQ6370B).

First, we generated 12.5 GHz grid-aligned converted signals according to ITU-T G.964.1. We fixed the original signal at a wavelength of 1551.72 nm with a power of −5.5 dBm, and changed the wavelength of the pump in steps of 6.25 GHz with a power of 3.5 dBm. The bias current of the SOA was set to 280 mA. Here, we take the QPSK signal as an example of the signal spectra after FWM in Fig. 10(a)–(d). The wavelengths of the four converted idlers are 1550.91 nm, 1550.81 nm, 1550.71 nm, and 1550.61 nm. We then increased the frequency detuning between the pump and the original signal to 500 GHz, so that the conversion range increased to 1 THz at steps of 200 GHz, as shown in Fig. 10(e)–(h). We can see that the larger conversion range leads to a lower optical signal noise rate (OSNR), which is related to the conversion efficiency (CE). To achieve the optimal FWM conversion efficiency, the pump and input signal are adjusted to the co-polarized states using the PCs [17].

Then, we measured the OSNR of the converted signal as a function of conversion range for DPSK, QPSK, and 16QAM, respectively. Here, we also took the QPSK signal as example to measure the OSNR curve at the step of 12.5 GHz. With the help of tunable lasers, finer-grid WSS, and flat-gain SOA, the converted 12.5 GHz grid-aligned signal was achieved, as shown in Fig. 11(a). The OSNRs of DPSK and 16QAM were also measured at the step of 100 GHz and the OSNR curves were fitted. From Fig. 11(a), it was seen that three kinds of curves were almost overlapped, which implies that three kinds of signals with the same input power display the similar OSNR performance. In addition, we investigated the influence of bias current on CE. The bias current was set from 240 to 340 mA and other conditions were kept. We selected four converted signals at the different

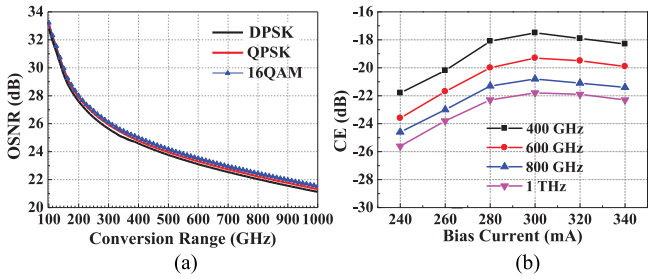

Fig. 11. Conversion effect. (a) OSNR of the converted signal as a function of conversion range. (b) CE as a function of bias current.

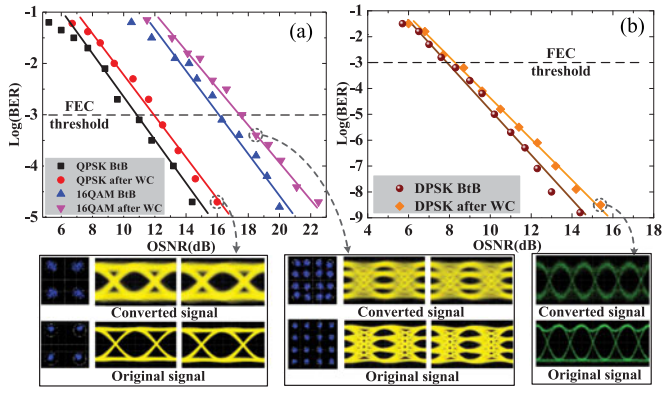

Fig. 12. BER performance as a function of OSNR for (a) QPSK and 16QAM. (b) DPSK. (Insets) Corresponding constellations and eye-diagrams.

conversion ranges to analyze the effect of bias current on CE, as shown in Fig. 11(b). When the bias current was small, the CE was improved as the bias current rised. That was because larger bias current provided higher carrier density which led to higher CE. However, when the bias current reached a certain value, the CE started to deteriorate as bias current rises. It was mainly because too large bias current might generate high-order FWM components and induced more ASE noise. The high-order FWM idlers consumed the energy from pumps and current, which led to a decline in CE. Moreover, the high-order FWM might cause the crosstalk to the converted signal which might further damage the signal performance. Fig. 11(b) presented the optimum value of bias current was 300 mA.

Next, the BER performance was measured as a function of OSNR for the converted QPSK and 16QAM signals, as shown in Fig. 12(a). The original signals were also tested under a back-to-back (BtB) scenario for comparison. We chose the conversion range at 8 nm (1 THz) for this measurement, because larger conversion detuning not only satisfies practical EON applications, but also provides 22 dB OSNR, which is required to obtain the proper BER values. In addition, we also investigated the DPSK signal, as shown in Fig. 12(b). It can be observed that, for QPSK and 16QAM, the BER is lower than the FEC threshold of 10^{-3}, and compared with their own BtB cases, the OSNR penalties are less than 1.5 dB. For DPSK, owing to the on-line calculation, the BER can be tested to as low as 10^{-9}, meaning that error-free performance is achieved, and the OSNR penalty is less than 1 dB. The constellations and eye-diagrams of the original and converted signals are displayed in the insets of Fig. 12. Concentrated constellations and clear opening eye-diagrams confirm the acceptable performance of the conversion process and demonstrate the complete transparency of the scheme when applied to multilevel formats, even in the case of large conversion ranges.

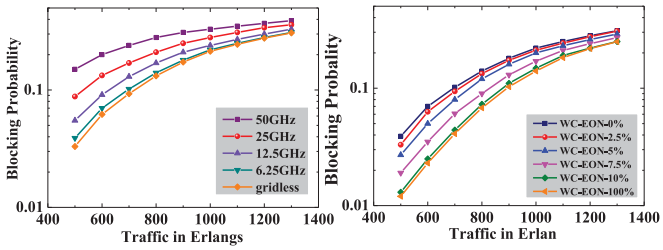

Fig. 13. Blocking probability as a function of traffic load. (a) Under different grid granularities. (b) With limited converters per node.

However, the lower-order format has better resistance to deterioration. Because of its longer Euclidean distance, DPSK signals are more robust in terms of OSNR degradation. From Fig. 12, we can see that, to achieve the same BER value, the higher order format requires a higher OSNR. Moreover, if we implement the same conversion range, the higher-order format exhibits worse BER characteristics, especially for long distance signals that suffer from accumulated dispersion and nonlinear noise. Therefore, in practical WC-EONs, the conversion range and transmission distance for different formats should be considered.

To investigate how the finer-grid WSS can be effectively used to improve the performance of EON, we also studied the control and management layer. We modified an effective routing, wavelength assignment, and spectrum allocation (RWSA) algorithm specifically for WC-EON [18]. We simulated the modified algorithm on the 14-node NSFNET topology. The network can support various line rates with the corresponding spectral widths. First, we measured the blocking performance of the non-wavelength convertible networks under different grid granularities (i.e., 50 GHz, 25 GHz, 12.5 GHz, 6.25 GHz, and gridless), as shown in Fig. 13(a). It is seen that the blocking performance improves as the grid granularity decreases, resulting in a lower blocking probability. Another interesting observation is the performance saturation phenomenon. When the grid granularity decreases to a certain level (in this case, 6.25 GHz), the overall blocking performance of the finer-grid case is similar to that in the gridless case. Thus, the finer-grid EON based on our WSS can optimize the network performance, but it would appear that there is no need to over-enhance the tuning resolution of optical components, as little improvement is observed when the tuning resolution is less than 6.25 GHz.

Finally, we measured the blocking performance of the 6.25 GHz grid EON with different levels of WC capacity, as shown in Fig. 13(b). The upper curve shows the non-wavelength convertible case, and the lower curve shows the full wavelength conversion capacity. The middle curves represent the blocking performance of EON with a shared WC module, which means only certain requests can implement the WC function. It can be seen that the blocking probability improves with the proportion of WC capacity at a node. However, after deploying only 10% of the total number of requests, the blocking probability remains stable and is very close to the network with full WC capacity. Thus, though WC can further improve the network performance, the advantages of full WC capacity can be achieved by investing in a small percentage of converters, which demonstrates the effectiveness of our proposed shared AOWC module.

5. Conclusion

In conclusion, we have proposed and fabricated an LCoS-based WSS. Compared with the conventional WSS, based on the cost-effective method, namely combined lenses technique, the proposed WSS offers improved bandwidth setting resolution and enhanced grid granularity of 6.25 GHz. To achieve finer-grid WSS, we preferred to increase the focal length rather than decrease the pixel size of LCoS. The advantage of our technique was that the focal length of combined lenses could be adjusted flexibly by changing the distance between two cylinder lenses, by neither damaging the

aberration nor increasing additional cost. Aimed at NG-EON, we conducted physical experiments to test the finer-grid WSS-based AOWC module, which demonstrated that AOWC was feasible for DPSK, QPSK, and 16QAM signals. In addition to physical experiments, a network simulation for the corresponding control and management scheme was also performed. The results show that the finer-grid WSS effectively increases the spectrum efficiency, improves the conversion resolution, and decreases the blocking probability, demonstrating the feasibility of the finer-grid WSS and AOWC for future EONs.

Finally, based on above the proposed 1 $\times$ 9 WSS, the key techniques, including WSS bandwidth resolution setting, LCoS beam deflection, and Gauss beam transformation, have the potential to be applied for the development of $M \times N$ WSS, which is the essential component for ROADM contentionless implementation, and will be further researched in the future.

References

[1] D. Yu, S. Fu, Z. Hong, M. Tang, P. Shum, and D. Liu, "Characterization and mitigation of phase-modulation-dependent loss of liquid crystal on silicon." *Opt. Lett.*, vol. 40, no. 7, pp. 1484–1487, 2015.

[2] M. Salsi, C. Koebele, D. Sperti, and P. Tran, "Mode-division multiplexing of 2 100 gb/s channels using an LCoS-based spatial modulator," *J. Lightw. Technol.*, vol. 30, no. 4, pp. 618–623, Feb. 2012.

[3] F. Peng, Y. H. Lee, Z. Luo, and S. T. Wu, "Low voltage blue phase liquid crystal for spatial light modulators." *Opt. Lett.*, vol. 40, no. 21, pp. 5097–5100, 2015.

[4] Y. Sakurai *et al.*, "LCoS-based wavelength blocker array with channel-by-channel variable center wavelength and bandwidth," *IEEE Photon. Technol. Lett.*, vol. 23, no. 14, pp. 989–991, Jul. 2011.

[5] K. Sorimoto *et al.*, "Compact and phase-error-robust multilayered AWG-based wavelength selective switch driven by a single LCoS," *Opt. Exp.*, vol. 21, no. 14, pp. 17131–17149, 2013.

[6] G. Shen and Q. Yang, "From coarse grid to mini-grid to gridless: How much can gridless help contentionless?" in *Proc. Opt. Fiber Commun. Conf. Expo./Nat. Fiber Opt. Eng. Conf.*, 2011, pp. 1–3.

[7] O. Gerstel, M. Jinno, A. Lord, and S. J. B. Yoo, "Elastic optical networking: A new dawn for the optical layer?" *IEEE Commun. Mag.*, vol. 50, no. 2, pp. s12–s20, Feb. 2012.

[8] *Spectral Grids for WDM Applications: DWDM Frequency Grid*, ITU-T G.694.1, 2012.

[9] M. A. Roelens, J. B. Schroeder, P. Blown, C. Pulikkaseril, S. Poole, and S. Frisken, "Applications of LCoS-based programmable optical processors," in *Proc. Opt. Fiber Commun. Conf.*, 2014, Art. no. W4F-3.

[10] C. Lim, C. Pulikkaseril, and K. L. Lee, "A study on LCoS-based remote nodes for 60 GHz fiber-wireless links," *J. Lightw. Technol.*, vol. 30, no. 19, pp. 3110–3117, Oct. 2012.

[11] A. N. Patel, P. N. Ji, J. P. Jue, and T. Wang, "Routing, wavelength assignment, and spectrum allocation in wavelength-convertible flexible optical WDM (WC-FWDM) networks," in *Proc. Nat. Fiber Opt. Eng. Conf.*, 2012, Art. no. JTh2A-36.

[12] D. Wang, M. Zhang, J. Qin, G.-W. Lu, H. Wang, and S. Huang, "Multifunctional switching unit for add/drop, wavelength conversion, format conversion, and WDM multicast based on bidirectional LCoS and SOA-loop architecture," *Opt. Exp.*, vol. 22, no. 18, pp. 21847–21858, 2014.

[13] D. Wang *et al.*, "Multifunctional all-optical signal processing scheme for simultaneous multichannel WDM multicast and XOR logic gates based on FWM in QD-SOA," in *Proc. Opt. Fiber Commun. Conf.*, 2015, Art. no. Th2A–5.

[14] D. Wang, M. Zhang, Z. Li, and Y. Cui, "Flexible optical cross-connect structures supporting WDM multicast with multiple pumps for multiple channels," *IEEE Photon. J.*, vol. 6, no. 6, pp. 1–12, Dec. 2014.

[15] S. Gringeri, B. Basch, V. Shukla, R. Egorov, and T. J. Xia, "Flexible architectures for optical transport nodes and networks," *IEEE Commun. Mag.*, vol. 48, no. 7, pp. 40–50, Jul. 2010.

[16] A. N. Patel, P. N. Ji, J. P. Jue, and T. Wang, "On-line routing, wavelength assignment, and spectrum allocation in wavelength convertible flexible optical WDM networks," *Proc. SPIE*, vol. 8283, no. 3, pp. 579–590, 2012.

[17] J. P. R. Lacey, M. A. Summerfield, and S. J. Madden, "Tunability of polarization-insensitive wavelength converters based on four-wave mixing in semiconductor optical amplifiers," *J. Lightw. Technol.*, vol. 16, no. 12, pp. 2419–2427, Dec. 1999.

[18] A. N. Patel, P. N. Ji, and J. P. Jue, "Routing, wavelength assignment, and spectrum allocation in wavelength convertible flexible optical wavelength-division multiplexing networks," U.S. Patent 8 909 043, Dec. 9, 2014.